

Moderate Temperature Clusters of Galaxies from the RDCS and the High Redshift Luminosity–Temperature Relation.^{1,2,3}

B. P. Holden^{4,5}, S. A. Stanford^{4,5}

Department of Physics, University of California, Davis, CA 95616

bholden@igpp.ucllnl.org, adam@igpp.ucllnl.org

G. K. Squires⁵

SIRTF Science Center, California Institute of Technology, Pasadena, CA 91125

squires@ipac.caltech.edu

P. Rosati⁵

European Southern Observatory, Karl-Schärzschild-Strasse 2, D-85748 Garching, Germany

prosati@eso.org

P. Tozzi

Osservatorio Astronomico di Trieste, via G.B. Tiepolo 11, I-34131, Trieste, Italy

tozzi@ts.astro.it

P. Eisenhardt

Jet Propulsion Laboratory, California Institute of Technology, MS 169-327, 4800 Oak Grove Drive, Pasadena, CA 91109

prme@kromos.jpl.nasa.gov

and

H. Spinrad

¹Based in part on observations obtained at the W.M. Keck Observatory

²Based in part on observations obtained at Palomar Observatory

³Based in part on observations obtained with the Chandra X-ray Observatory

⁴Participating Guest, Institute of Geophysics and Planetary Physics, Lawrence Livermore National Laboratory

⁵Visiting Astronomer, Kitt Peak National Observatory, National Optical Astronomy Observatory, which is operated by the Association of Universities for Research in Astronomy, Inc. (AURA) under cooperative agreement with the National Science Foundation.

Astronomy Department, University of California, Berkeley, CA 94720

`spinrad@bigz.berkeley.edu`

ABSTRACT

We present our discovery observations and analysis of RDCS1317+2911, $z = 0.805$, and RDCS1350+6007, $z = 0.804$, two clusters of galaxies identified through X-ray emission in the **ROSAT** Deep Cluster Survey (RDCS). RDCS1317+2911 has an unusual morphology in our **Chandra** observations, with an asymmetric surface brightness profile and a bend in the distribution of X-ray emission. In contrast, RDCS1350+6007 appears to be more like low redshift clusters, with $\beta = 0.49 \pm 0.06$ and $r_{core} = 165 \pm 5$ kpc ($\Omega_m = 0.3$, $\Omega_\Lambda = 0.7$, $H_0 = 65$ km s $^{-1}$ Mpc $^{-1}$), though it also has an elliptical, slightly asymmetric surface brightness profile. We find a temperature of $3.7_{-0.9}^{+1.5}$ keV and a bolometric luminosity of $8.2_{-1.6}^{+1.7} \times 10^{43}$ erg s $^{-1}$ for RDCS1317+2911, and a temperature of $4.9_{-0.9}^{+1.3}$ keV and a bolometric luminosity of $4.1_{-0.4}^{+0.5} \times 10^{44}$ erg s $^{-1}$ for RDCS1350+6007. Our weak lensing analysis of RDCS1350+6007 confirms the general shape of the inner density profile but predicts twice the mass of the model based on the X-ray profile. There are two possibilities for this discrepancy, either there is a significant amount of mass near the redshift of the cluster that has not yet fallen into the potential well and shock heated the gas, or, as we only see the X-ray emission from the core of the cluster, our β model fails to describe the true shape of the underlying potential.

We combine the X-ray luminosities and temperatures for RDCS clusters of galaxies with such measurements of other clusters at high redshift ($z > 0.7$) and fit the luminosity-temperature relation. We find no statistically significant evolution in the slope or zero-point of this relation at $z_{median} = 0.83$. This result is in agreement with models of intracluster medium evolution with significant pre-heating or high initial entropy values. Quantifying the bolometric luminosity-temperature relation as $L = L_6(1+z)^A(T/6\text{keV})^\alpha$, we find $alpha = 2.9 \pm 0.4$, $L_6 = 8.7 \pm 0.9 \times 10^{44}$ erg s $^{-1}$ and $A = 0.3 \pm 0.2$, or $A = 0.4 \pm 0.2$, depending on which low redshift luminosity temperature relation we compare with. With this result, we rule out at the 5σ level the self-similar scaling model of intracluster medium evolution. We discuss how low temperature, high redshift clusters of galaxies will allow us to improve on this result and announce the discovery of two such objects, CXOU J0910.1+5419 and CXOU J1316.9+2914.

Subject headings: galaxies: clusters: general — catalogs — cosmology: observations — galaxies: clusters: individual (RDCS1350+6007, RDCS1317+2911, CXOU J0910.1+5419, CXOU J1316.9+2914) — X-rays

1. Introduction

The luminosity-temperature relation for clusters of galaxies has presented a puzzle for a number of years. Using simple analytical scaling relations, Kaiser (1986) found that X-ray luminosity of clusters of galaxies should scale as $L_x \propto T_x^2$. However, since the first compilations of the luminosities and temperatures for clusters of galaxies (Edge & Stewart 1991, for example), it has been clear that $L_x \propto T_x^{2.6-3.0}$, a steeper relation than predicted.

One way to break the scaling laws that predict $L_x \propto T_x^2$ is to have non-gravitational energy injected into the intracluster medium (ICM) before or during cluster formation. This solution, called pre-heating, was originally invoked to solve two related problems. Kaiser (1991) and Evrard & Henry (1991) used pre-heating to explain the apparent negative evolution of the X-ray cluster luminosity function (Gioia et al. 1990; Henry et al. 1992) from the Einstein Medium Sensitivity Survey in an $\Omega_m = 1$ Universe. White (1991) also used pre-heating, in the form of supernovae-driven galactic winds, to explain why groups and low mass clusters seem to have higher X-ray temperatures than expected based on galaxy member velocity dispersions, or $1 < \beta_{spec} \propto \frac{\sigma_v^2}{T_x}$. This is the same sort of behavior observed for the luminosity-temperature relation where the temperature is too high for the luminosity when compared with the highest temperature systems (Helsdon & Ponman 2000). Recently Ponman et al. (1999) showed clearly that the entropy of the ICM in the center of low temperature clusters is greater than the value expected from gravitational collapse. Many authors have shown that this additional entropy can reproduce many X-ray observational properties (Bower et al. 1997; Cavaliere et al. 1997, 1999; Lloyd-Davies et al. 2000; Loewenstein 2000; Wu et al. 2000; Tozzi & Norman 2001; Bialek et al. 2001; Borgani et al. 2001a; Voit & Bryan 2001, for example). However, there are many different physical processes that could break the simple self-similar scaling, including heating from SN or from AGN, or the removal of low entropy gas via cooling (Voit & Bryan 2001, for example). To distinguish among these processes, the observations of high z groups and clusters to measure the evolution in the observed scaling relations as a function of redshift will prove crucial.

In order to tackle the thermal evolution of the ICM, we are examining the highest redshift sample of X-ray selected clusters of galaxies known, the **ROSAT** Deep Cluster Survey (Rosati et al. 1998, RDCS). Our goal is to observe all of the $z > 0.8$ clusters in this catalog with the Chandra (O'dell & Weisskopf 1998) and XMM-Newton, thus creating a flux limited sample at high redshifts with high quality ICM temperature and luminosity measurements. This will enable us to study both the luminosity-temperature relation and to determine the distribution functions of both of those physical measurements. In this paper we discuss our results for two clusters of galaxies from the RDCS, RDCS1317+2911 in §2 and RDCS1350+6007 in §3. We then combine these data with our other observations of $z > 0.8$ RDCS clusters of galaxies, along with a number of other high redshift clusters, and examine the luminosity-temperature relation in §4. In §5, we discuss the lack of measured evolution of the luminosity-temperature relation and discuss how future surveys can improve upon our understanding of the thermal history of the ICM. We use $H_0 = 65 \text{ km s}^{-1} \text{ Mpc}^{-1}$, $\Omega_m = 0.3$, and $\Omega_\Lambda = 0.7$. At the redshifts of RDCS1317+2911 and RDCS1350+6007, this cosmol-

ogy corresponds to approximately 8 kpc per second of arc. Unless otherwise noted, errors represent 68% confidence limits.

2. RDCS1317+2911

2.1. Optical and Near-Infrared Data

Our optical data for RDCS1317+2911 are a 1200 second I band from January, 1996 using the Mayall 4m telescope with the Mosaic Imager, and an 1880 second Thuan-Gunn i band image using COSMIC (Kells et al. 1998) on the Palomar 5m telescope. For the Palomar data, we had moderate seeing, full-width at half-maximum $\simeq 1''.2$, in non-photometric conditions. The data covered a $9''.7$ by $9''.7$ field of view with $0''.2856$ pixels. We observed this cluster in J and K_s with the Prime Focus IR Camera (Jarrett et al. 1994) with the Palomar 5m in photometric conditions on 1998 March 24. This camera provides a $2''.1$ field of view with $0''.494$ pixels. The flux scale was calibrated using observations of three UKIRT standard stars obtained on the same night. The data were taken using a sequence of dither motions with a typical amplitude of $15''$ and a dwell time between dithers of 30 seconds. The data were linearized using an empirically measured linearity curve, and reduced using DIMSUM⁶. In Figure 1, we show a color-composite image from these data with the blue component from the I band data, the green from the J and the red from the K_s data.

A catalog of objects in the K_s -band image was obtained using SExtractor (Bertin & Arnouts 1996) after first geometrically transforming the K_s and J images to match the I -band frame. The resolution of the IR images was also degraded slightly to match that of the I -band image. Objects were detected on the K -band image with the requirement that the object covers an area of 0.78 arcsec 2 and must be 1.5σ above the background. For reference the 3σ detection limit is $K \sim 21.3$ in the 2 arcsec aperture used to measure colors. All detected objects down to this limit were inspected visually to eliminate false detections. The catalog was then applied to the J and I band images to obtain matched aperture photometry.

From these data we made color-magnitude diagrams, shown in Figure 2. In both colors, there is a clear red sequence of galaxies, many of which are apparent in Figure 1. We used the color-magnitude diagrams to choose targets for slit mask observation. RDCS1317+2911 was observed using the Low Resolution Imaging Spectrograph (Oke et al. 1995, LRIS) on the Keck I telescope. We obtained the spectra using LRIS with a 150 line mm $^{-1}$ grating blazed at 7500 Å, which has a dispersion of 4.8 Å pixel $^{-1}$. The mask was observed in June of 1999 for three exposures of 1800 seconds with small offsets along the slits between exposures.

We reduced the two-dimensional data using a set of IRAF⁷ scripts optimized for LRIS ob-

⁶Deep Infrared Mosaicing Software, a package of IRAF scripts available at <ftp://iraf.noao.edu/contrib/dimsumV2>

⁷The Image Reduction and Analysis Facility (IRAF) software is provided by the National Optical Astronomy

servations. These scripts greatly reduce the fringing evident in LRIS spectra at long wavelengths when used on dithered observations. We extracted one-dimensional spectra using the IRAF package APEXTRACT. Individual redshifts were measured by fitting the positions of lines and the 4000Å break.

We found six galaxies with $0.798 < z < 0.810$, which are circled in Figure 2. We show these spectra in Figures 3 and 4, plotted in the rest-frame of the cluster. We show, in addition, four vertical dashed lines representing the break at 2900 Å, the break at 3260 Å, O II at 3727 Å, and the break at 4000 Å. Using the biweight center (Beers et al. 1990), we found $z = 0.805 \pm 0.002$ for the cluster. We estimated the errors using the jackknife of the biweight center as recommended in Beers et al. (1990).

2.2. X-ray Data

RDCS1317+2911 was observed by *Chandra*, using ACIS-I, as part of our program to study the physical properties of the ICM in all $z > 0.8$ RDCS clusters. RDCS1317+2911 was observed for an effective exposure time of 111.3 ks (Obs ID 2228) on May 4th and 5th, 2001. The observation was done with the very faint mode when ACIS was operating at a temperature of -120 C.

We processed the Level 1 data for each observation using the CIAO v2.1.3 software. We cleaned the Level 1 event list for all events with ASCA grades of 1, 5 and 7, filtered the data not in good time intervals, removed bad offsets and removed bad columns. In addition, we used the routines in clean55.1.0 (Vikhlinin 2001) to remove particle background events from data taken with the very faint mode.

We then removed, on a chip by chip basis, 3.3 second time intervals when the count-rate exceeded three standard-deviations above the average count-rate, *i.e.* $\simeq 1.25$ counts per second. Once we had created clean event files and corresponding exposure maps, we merged the chip by chip event lists into one event file for the whole pointing. For the Level 1 processing, we used the ACIS calibration files that were available on June 1, 2001.

2.3. X-ray Imaging Results

In Figure 1 we plot our 0.5-2.0 keV data for this cluster, smoothed with a 3'' Gaussian and overlaid on our ground based imaging. Overall, the cluster has a compact, highly elliptical shape. Using the Sherpa software package (Freeman et al. 2001), we fit an elliptical β model to the 0.5-2.0 keV photons. The resulting model had a core radius of 0''.1, and $\beta = 0.34$ with an ellipticity $\epsilon = 0.53$

Observatories (NOAO), which is operated by the Association of Universities of Research in Astronomy for Research in Astronomy, Inc., under contract to the National Science Foundation.

and is centered at $\alpha = 13h17m21\overset{s}{.}70$ $\delta = +29^\circ11'18\overset{''}{.}1$ (J2000). The errors on all of these parameters are too small, $\sim 1\%$ and the parameters appear quite different when compared with lower redshift clusters of galaxies (Jones & Forman 1999). This is because the model does not describe the data well. As seen in Figure 1, the X-ray emission from the cluster is not symmetric but rather appears to have a strong kink. Also, the peak in the X-ray emission is off-center. When we examine the difference between the smoothed data and the best fitting model smoothed with the same Gaussian, there is a clear over subtraction by the model in the center and an under subtraction at the edges.

We measured an X-ray temperature for RDCS1317+2911 in the manner of our other Chandra observations of RDCS clusters (Stanford et al. 2001; Holden et al. 2001; Stanford et al. 2002). First we placed a circular aperture of $30''$ over the center of the cluster as determined from the peak of the X-ray emission. We removed point sources from that aperture, including the hard X-ray source shown in the inset of Figure 1. For a background region, we extracted two rectangular apertures on either side of the circular aperture. For each background region, we also removed point sources. The two background regions were constructed to have almost all of the flux land on the same node of the CCD as the cluster. For the background, we constructed weighted response matrix files and auxiliary response matrix files using Alexey Vikhlinin’s `calcarf/calcrmf` tools (which have become part of the 2.2 version of the CIAO package). We fit the background regions using the `XSPEC` package of Arnaud (1996) using a single component power law not convolved with the auxiliary response matrix as a model for the background from 0.5-6.0 keV with the addition of Gaussian at 2.1 keV to model the Au emission line. Both regions were fit simultaneously with only the normalizations allowed to vary.

We fit the data inside the $30''$ aperture using the Cash statistic (Cash 1979) with a Raymond-Smith model (Raymond & Smith 1977) and the above background model after rescaling for the relative areas. There were a total of 313 events in the energy range of 0.5-6.0 keV. We expected 137.7 events in the same energy range from the background. The small number of events in the cluster, 175.3 net events, means we cannot constrain the abundance or redshift from our data. We, therefore, assumed a metal abundance of 0.3 solar (Horner et al. 2001) and a redshift of $z = 0.805$ for the cluster. We included a galactic absorption of $1.0 \times 10^{20} \text{ cm}^{-2}$ (Stark et al. 1992). We found the best fitting temperature to be $3.7^{+1.5}_{-0.9}$ keV. We found, inside the aperture, a flux of $6.5^{+0.6}_{-0.6} \times 10^{-15} \text{ ergs cm}^{-2} \text{ s}^{-1}$ (0.5-2.0 keV) and $1.1^{+0.1}_{-0.1} \times 10^{-14} \text{ ergs cm}^{-2} \text{ s}^{-1}$ (0.5-6.0 keV). We plot our best fitting spectrum in Figure 5 with the background model subtracted and the data grouped into bins of 10 events each. Given the poor fit using the β model, we used a curve of growth from the 0.5-2.0 keV band to determine the total flux. Beyond a radius of $80''$, the total flux remains flat. We find a total luminosity within 1 Mpc, $125''$, of $3.0^{+0.6}_{-0.6} \times 10^{43} \text{ erg s}^{-1}$ (0.5 - 2.0 keV, in the rest frame of the cluster) and $8.2^{+1.7}_{-1.6} \times 10^{43} \text{ erg s}^{-1}$ bolometric.

Our errors are computed by 1000 Monte Carlo simulations using the combined background and Raymond-Smith models. For each simulation, we use the `XSPEC` `fakeit` command to make a simulated source with background spectrum. The same fitting process used for the real data is then performed. The errors are estimated from the distribution of the resulting temperature, flux

and luminosity values. The median temperature, flux and luminosity values agreed with the input values.

We also fit a power law model to the hard X-ray source in the core of the cluster. This source looks like a potential cluster member based on the colors of the galaxy aligned with the X-ray emission but currently it does not have a redshift. As this hard source sits on top of the cluster X-ray emission, we removed both the background and the cluster emission when determining the spectrum. We estimate a flux of $1.1_{-0.2}^{+0.2} \times 10^{-15}$ ergs $\text{cm}^{-2} \text{ s}^{-1}$ (0.5-2.0 keV) and $8.7_{-2.1}^{+2.4} \times 10^{-15}$ ergs $\text{cm}^{-2} \text{ s}^{-1}$ (2.0-10.0 keV) with a power-law slope of 0.6 ± 0.3 for the source.

3. RDCS1350+60

3.1. Optical and Near-Infrared Data

The optical counterpart for RDCS1350+6007 was originally observed using the Mayall 4m Telescope with an *I* band exposure. Using that data, a mask was made for the CryoCam spectrograph on the Mayall 4m Telescope and three redshifts were measured in the cluster with $z = 0.809$, $z = 0.808$ and $z = 0.799$ from spectra taken in April, 1996. Two masks for LRIS were made via visual selection using the Kitt Peak *I* band image taken for the initial cluster discovery. We observed each mask twice with LRIS for 1200 seconds, with offsets between each observation. We took our spectra in June of 1999 using the 150 line mm^{-1} grating blazed at 7500 Å. We show an image of the cluster in Figure 6.

The cluster redshift for RDCS1350+6007 was determined by searching for peaks in the redshift distribution that consisted of galaxies close to the X-ray centroid. There are seven galaxies in the redshift range $0.800 < z < 0.809$ that are likely cluster members. We used the same procedure as we used for RDCS1317+2911 and find $z = 0.804 \pm 0.002$ for the redshift of RDCS1350+6007. We show those spectra in Figures 7 and 8. Three galaxies in this set of spectra were also those observed with CryoCam. All three objects had the same measured redshift in the LRIS spectra as was originally found in the Cryocam data.

RDCS1350+6007 was observed June, 1999 for 9300 seconds with LRIS in the *R* band in $0''.6$ seeing. These data were used as the blue color in the image in Figure 6. Our *J* and *K* data, green and red in Figure 6 respectively, were acquired with the Simultaneous Quad IR Imaging Device (Ellis et al. 1992, SQIID) on the KPNO Mayall 4 meter telescope. We observed RDCS1350+6007 for 4080 seconds in June of 2001. The instrument has $0''.39$ pixels and, as its name implies, takes *J*, *H*, *K* and *L* data simultaneously. We use only the *J* and *K* data in this paper. The data were taken using a sequence of dither motions with a typical amplitude of $15''$ and a dwell time between dithers of 120 seconds. The data were reduced using DIMSUM. Using SExtractor, objects were detected in the *K*-band image with the requirement that the object covers an area of 0.8 arcsec^2 and must be 1.5σ above the background. For computing colors, a $3''.3$ aperture was used and a 5σ

detection in that aperture is $K = 20.0$. We plot the color-magnitude diagrams for RDCS1350+6007 in Figure 9. The circled objects are galaxies with redshifts in the cluster. Those points with squares around are galaxies with redshifts that lie outside the cluster.

3.2. X-ray Results

RDCS1350+6007 was observed for an effective exposure time of 58 ks on August 29th and 30th, 2001 (Obs ID 2229) with ACIS-I instrument on the **Chandra** X-ray Observatory. The observation and initial event screening was done using the same parameters as RDCS1317+2911 as discussed in §2.2.

Glancing at Figure 6, it is clear that RDCS1350+6007 has more extended X-ray emission and has a much higher X-ray luminosity than RDCS1317+2911. In Figure 6 we plot our 0.5-2.0 keV data for this cluster, smoothed with a 3'' Gaussian and overlaid on our ground based imaging. Once again, using the Sherpa package, we fit an elliptical β model to the 0.5-2.0 keV photons. The resulting model had a core radius of $20.3' \pm 0.5'$ and $\beta = 0.49 \pm 0.06$ with an ellipticity $\epsilon = 0.39 \pm 0.03$ with an X-ray centroid at $\alpha = 13h50m48.55s$ $\delta = +60^\circ 07' 06.7''$ (J2000). Other than the high ellipticity, there is nothing unusual about these model parameters. The value for β lies within the observed distribution of Jones & Forman (1999) but does create a problem. At large radii, a β profile has the observed distribution of $\propto (\frac{r}{r_c})^{-6\beta+1}$, which, with our measured value of β , yields a surface brightness profile $\propto (\frac{r}{r_c})^{-2}$. This means that the integrated flux of cluster increases logarithmically with radius so we cannot use the β model to calculate an aperture correction for a total luminosity at an infinite radius. Instead, we compute the total luminosity at a radius of 1 Mpc as with RDCS1317+2911.

For RDCS1350+6007 we measured the X-ray temperature and flux inside an ellipse described by the best fitting β model with the events taken from within one core radius. The one issue with this approach is that, as shown in Figure 6, the cluster is asymmetric with more flux to the south-east than to the north-west of the cluster centroid. As with RDCS1317+2911, we extracted a background region and fit a model to the background region. We chose a slightly more complicated model consisting of a Gaussian and a broken power law⁸ not convolved with the auxiliary response matrix and we fit the energy range of 0.8-6.0 keV. We chose 0.8 keV for our cutoff in the energy range instead of 0.5 keV because of a noticeable change in our background regions below that energy. To fit this change would require a much more complicated background model than the broken power law and single Gaussian we used.

We rescaled the normalization of the background model and fit the cluster events with a Raymond-Smith model with a galactic absorption of $1.8 \times 10^{20} \text{ cm}^2$ (Stark et al. 1992). In this

⁸A broken power law consists of two power law models with a shared normalization, for three free parameters. The two components meet at a specific energy, the fourth parameter of the model.

aperture we found 354 events from 0.8 keV to 6.0 keV, the energy range we fit the data and background over, while we expected 58 events from the background in the aperture. Freezing the redshift at $z = 0.804$ and the metal abundance at 0.3 solar, we found the temperature to be $4.9_{-0.9}^{+1.3}$ keV. We plot our best fitting spectrum in Figure 10 with the background model subtracted and the data grouped into bins of five events each. The bump in the spectrum at $\simeq 3.7$ keV corresponds to the expected location of the 6.7 keV Fe feature. Inside the aperture, we find flux of $2.3_{-0.16}^{+0.16} \times 10^{-14}$ ergs cm $^{-2}$ s $^{-1}$ in the ROSAT hard band (0.5 - 2.0 keV) and $4.1_{-0.38}^{+0.38} \times 10^{-14}$ ergs cm $^{-2}$ s $^{-1}$ (0.5 - 6.0 keV). The luminosity is $1.4_{-0.2}^{+0.2} \times 10^{44}$ ergs s $^{-1}$ (0.5 - 2.0 keV, in the rest frame of the cluster) and $4.1_{-0.4}^{+0.5} \times 10^{44}$ ergs s $^{-1}$ (bolometric) within a radius of 1 Mpc, using the β model to compute the flux inside that radius. Our errors are computed by 1000 Monte Carlo simulations, as was done for RDCS1317+2911, using the combined background and Raymond-Smith model. For the luminosity errors, we included our errors in the β model fit to the surface brightness distribution.

Because of the presence of the 6.7 keV Fe feature, we fit the data assuming a free redshift and abundance. We found a temperature of $4.7_{-1.0}^{+1.4}$ keV, an abundance of $0.44_{-0.24}^{+0.43}$ relative to solar and $z = 0.84_{-0.07}^{+0.03}$ which is in good agreement with our fixed values. Choosing an ellipse of two core radii, we found $4.1_{-0.5}^{+0.7}$ keV, an abundance of $1.06_{-0.37}^{+0.57}$ relative to solar and $z = 0.87_{-0.02}^{+0.01}$. This abundance is quite high but requires a redshift in disagreement with the redshifts measured with optical spectra. This apparently high abundance comes from a number of events with energies near the expected Fe feature. These events are not centrally concentrated like those events at the expected energy of the Fe feature given the optically measured redshift of the cluster. Therefore, we forced the redshift to agree with that of the optical spectra. That results in a temperature of $4.3_{-0.5}^{+0.7}$ keV and an abundance of $0.58_{-0.29}^{+0.40}$. For the rest of this paper we will use our results with a fixed abundance and redshift within one core radius, keeping the results from this cluster in agreement with RDCS1317+2911 as well as those in Stanford et al. (2001) and Stanford et al. (2002). Nonetheless, we note that this cluster has a higher than expected metal abundance.

3.3. Weak lensing Analysis

Using the 9300 second R band Keck/LRIS exposure discussed in §2.2, we modeled the mass distribution of RDCS1350+6007 based on the distribution of image shears of distant field galaxies caused by weak lensing from the cluster. The lensing analysis followed standard techniques, correcting for point spread function anisotropy following the Kaiser, Squires & Broadhurst method (Kaiser et al. 1995; Hoekstra et al. 1998), and calibrating losses due to seeing, pixelization, etc. as prescribed in Luppino & Kaiser (1997).

In order to compare the mass determined from the lensing with that inferred via a standard X-ray analysis, we adopted the following procedure. Based on the X-ray data, we assumed an isothermal sphere with a gas density profile given by a β model fit. In the X-ray data, we lacked the signal to compare to a more sophisticated elliptical model, so we employed only this circularly symmetric model. The weak-lensing analysis determines the mass in concentric cylinders along the

line of sight. To compare with the X-ray inferred mass, we re-fit a β model, but fixed the ellipticity to zero. The resulting β model has a core radius $15''.6 \pm 0''.4$, and $\beta = 0.50 \pm 0.02$. The core radius in the circularly symmetric model is smaller because the symmetric model cannot fit the light to the southeast of the core (see Figure 6).

In the spherical model, the total mass enclosed inside a radius filled with a gas in hydrostatic equilibrium, with density ρ_g and temperature T , is

$$M_{3D}(r) = -\frac{kT(r)}{\mu m_p G} \left[\frac{d \log \rho_g(r)}{d \log r} + \frac{d \log T(r)}{d \log r} \right] r \quad (1)$$

where r is the radius of interest, and μ is the mean molecular weight, which we set to be $\mu = 0.59$. An isothermal sphere with a β density profile yields the following mass distribution (Fabricant et al. 1984; Henry et al. 1993),

$$M_{3D}(r) = \frac{3\beta k T r_{core}}{\mu m_p G} \frac{(r/r_{core})^3}{1 + (r/r_{core})^2} \quad (2)$$

where $M_{3D}(r)$ is the mass enclosed within a sphere of radius r .

However, a few subtleties arise when comparing the X-ray inferred mass with that determined from the weak lensing analysis. First, the lensing returns the mass along the line of sight compared with the mass in a control aperture. Hence, we need to calculate the projected mass distribution from the parametric model fit to the X-ray data. Second, mass determinations from weak gravitational lensing analyses are necessarily lower estimates on the true mass along the line of sight. The observed shear is unperturbed by the addition of constant density sheets along the line of sight (Gorenstein et al. 1988). Furthermore, the relatively small field of view of these observations necessitates a differential determination of the total mass. This is facilitated by the statistic (Fahlman et al. 1994; Kaiser et al. 1995)

$$\begin{aligned} \zeta_{WL}(\theta_1, \theta_2) &= 2(1 - \theta_1^2/\theta_2^2)^{-1} \int_{\theta_1}^{\theta_2} d \ln(\theta) \langle \gamma_t \rangle \\ &= \bar{\kappa}(\theta_1) - \bar{\kappa}(\theta_1 < \theta < \theta_2) \end{aligned} \quad (3)$$

which measures the mean dimensionless surface density, κ , interior to radius θ_1 , relative to the mean in an annulus $\theta_1 < \theta < \theta_2$, and depends only on the measured galaxy shear estimates, γ_t .

In order to do a meaningful comparison between the X-ray and lensing mass determinations, we calculated an analogous estimator for the X-ray model as follows: From equation 2, we find the total mass density distribution (Fabricant et al. 1984; Henry et al. 1993) to be

$$\rho_{tot} = \frac{3\beta k T}{4\pi \mu m_p G r_{core}^2} \frac{3 + (r/r_{core})^2}{[1 + (r/r_{core})^2]^2}. \quad (4)$$

Hence, the projected mass density is given by

$$\Sigma_X(b) \equiv \int_{-\infty}^{\infty} \rho_{tot}(b, z) dz \quad (5)$$

$$= \frac{3\beta k T}{4G\mu m_p r_c} (1 + b^2/r_c^2)^{-3/2} \times \left(2 + \frac{b^2}{r_c^2} \right) \quad (6)$$

where b is the distance from the cluster center in the plane of the sky, and the z-axis defines the line-of-sight. The equivalent X-ray inferred mean (dimensionless) surface density interior to a given impact parameter, b , relative to the mean in a control region $b \leq b' \leq b_{\max}$ is given by

$$\zeta_X(b, b_{\max}) = \frac{3\beta kT}{2\mu m_p G r_c} (1 - b^2/b_{\max}^2)^{-1} \times \left[(1 + b^2/r_c^2)^{-1/2} - (1 + b_{\max}^2/r_c^2)^{-1/2} \right] / \Sigma_{\text{crit}}. \quad (7)$$

From either the lensing or X-ray analysis, the projected mass at a given radius r is estimated as

$$M_{2D/WL,X}(r) = \Sigma_{\text{crit}} \times (\pi r^2) \times \zeta_{WL,X}(r, r_{\max}). \quad (8)$$

The quantity Σ_{crit} is defined by $\Sigma_{\text{crit}}^{-1} = 4\pi G \beta_l D_l$ where $\beta = \langle D_{ls}/D_s \rangle$, and the distances D_l, D_{ls}, D_s are the angular diameter distance to the lens, between the lens and the background source, and to the source, respectively. For this analysis, we use the photometric redshift distributions (Gwyn & Hartwick 1996; Gwyn 1999; Fernández-Soto et al. 1999) inferred for galaxies in the Hubble Deep Fields to estimate Σ_{crit} for the magnitude cuts selected for the galaxies in the lensing catalog.

We plot in Figure 11 the resulting radial, projected total mass distributions calculated from equation 8, in concentric cylinders along the line of sight. The points are the results from the lensing, while the lines show the X-ray model, adopting $\theta_c = 15''.6$, $\beta = 0.49$, $kT = 4.9$ keV, and $\mu = 0.59$. We plot the 68% confidence lines on either side of the solid line representing the results from the best fitting β model. The statistical uncertainty in the X-ray mass determinations was calculated propagating the errors in quadrature.

It is apparent that our mass model based on the X-ray profile does not predict as high a mass as does the weak lensing shear signal. At large radii, this result is expected, as we show in Figure 6. We have a non-azimuthally symmetric X-ray gas distribution. Therefore, our circularly symmetric X-ray model will underestimate the total mass by neglecting the X-ray emission to the southeast. However, even at the core, our methods do not agree. Weak lensing depends on the projected mass along the line of sight, so we could be observing a system with a significant mass in the foreground that cannot be seen in the X-ray emission. One such example of this is the cluster ZwCL 0024+17 where the gravitational arcs (Tyson et al. 1998) and weak lensing (Smail et al. 1997) imply a large mass near the cluster. However, the X-ray analysis of Böhringer et al. (2000) find a small core radius, $r_{\text{core}} = 51$ kpc ($H_0 = 65 \text{ km s}^{-1} \text{ Mpc}^{-1}$) and $\beta = (0.43 - 0.55)$ (68% confidence limits). Such small values of β and r_{core} imply a small binding mass. With the galaxy redshift measurements from Czoske et al. (2001), it is clear that ZwCL 0024+17 is a merger along the line of sight, thus explaining the large lensing mass but the small gas mass implied by hydrostatic equilibrium. Such a line of sight merger could explain our small value for β . A merger could “puff-up” the gas, causing a smaller value for β than required by hydrostatic equilibrium. Interpreting our results shows the importance of using multiple methods of studying a cluster to disentangle the underlying mass distribution such as in Zaroubi et al. (1998), Holden et al. (2001) or Zaroubi et al. (2001).

4. The $z \simeq 0.8$ Luminosity-Temperature Relation

When we combined the clusters from Stanford et al. (2001, 2002) with those in this paper, we have a total of five $z > 0.8$ clusters of galaxies with **Chandra** observations to date. We will use this RDGS sample in conjunction with other cluster measurements from the literature, to estimate the luminosity-temperature relation at $z \simeq 0.8$. All clusters are listed in Table 1. In Figure 12, we plot the luminosities and temperatures of the above clusters. The RDGS clusters are labeled with solid dots, RDGS J0152.7-1357 by an open square, RX J1053.7+5753 by a diamond, and all of the other clusters are represented by just error bars. RX J0152.7-1357 was observed using Beppo-SAX (Della Ceca et al. 2000), RX J1716+6708 with **ROSAT** and **ASCA** (Gioia et al. 1999), and RX J1053.7+5753 was observed with **XMM-Newton** (Hashimoto et al. 2002), so our plot uses different symbols for those clusters. All of the other clusters were observed with **Chandra**. We also show the low redshift group data from Helsdon & Ponman (2000) and the low redshift cluster luminosity-temperature relation from Markevitch (1998).

For low redshift clusters, there is a fair amount of agreement in the slope of the luminosity temperature relation. Allen & Fabian (1998) estimate the luminosity-temperature relation for a sample analyzed in a manner similar to ours, a single temperature, isothermal model for the cluster, which they refer to as Model A. The sample spans $0.0258 \leq z \leq 0.451$, with $z_{med} = 0.2045$. Parameterizing the relation as $T_x = PL_{x,bol}^Q$, Allen & Fabian (1998) find $Q = 0.325 \pm 0.061$, using the bivariate correlated errors and intrinsic scatter (BCES) algorithm from Akritas & Bershady (1996) for fitting models to quantities with errors in both the x and y values. Conventionally, the luminosity-temperature relation is described by $L_{x,bol}$ (erg s $^{-1}$) = $L_6(T_x/6 \text{ kev})^\alpha$ where L_6 is the luminosity of a 6 keV cluster. In this form, the best fitting slope from Allen & Fabian (1998) is $\alpha = 3.1 \pm 0.6$. Markevitch (1998) finds $\alpha = 2.64 \pm 0.16$ using a sample of $0.04 \leq z \leq 0.09$, with $z_{med} = 0.055$, clusters of galaxies that have been corrected for cooling flows. Arnaud & Evrard (1999) find a similar result, $\alpha = 2.88 \pm 0.15$ for a sample constructed assuming isothermal temperatures but with strong cooling flow clusters removed. This sample spans $0.0038 \leq z \leq 0.370$ with $z_{med} = 0.0522$.

Our sample is rather heterogeneous, containing a number of clusters that appear to have multiple components (MS 1054.4-0321, RX J1053.7+5753, & RDGS0152.7-1357). In addition, we have made no corrections for cooling flow clusters. This means that the results of Allen & Fabian (1998) are the most comparable. Using the data plotted in Figure 12, we fit the luminosity as a function of temperature over the temperature range of 1 to 10 keV and found $\alpha = 3.0 \pm 0.4$ and $L_6 = 8.7 \pm 0.9 \times 10^{44}$ erg s $^{-1}$ using the BCES method. This sample has a median redshift of $z_{med} = 0.83$. If we trim the two clusters at $0.7 < z < 0.8$, we find a steeper slope with $\alpha = 3.1 \pm 1.1$ and $L_6 = 8.2 \pm 1.0 \times 10^{44}$ erg s $^{-1}$ with $z_{med} = 0.86$. Given the large errors, both fits are compatible at the 1σ level with all of the low redshift estimates.

Assuming no evolution in the slope, we can instead look for a change in the value for L_6 . The normalization of the luminosity-temperature relation of Arnaud & Evrard (1999) is $L_6 =$

$6.8 \pm 0.5 \times 10^{44}$ erg s $^{-1}$ while Markevitch (1998) finds $L_6 = 7.4 \pm 0.6 \times 10^{44}$ erg s $^{-1}$ (converted to $H_o = 65$ km s $^{-1}$ Mpc $^{-1}$). Both normalizations are lower than ours, though not by a statistically significant amount. If we lower our slope to be the same as Arnaud & Evrard (1999) or Markevitch (1998), our values for the normalization of the luminosity-temperature relation are roughly two standard deviations higher.

5. Discussion

In Borgani et al. (2001b), the authors parameterize the evolution of the luminosity-temperature relation with $L_{x,bol}$ erg s $^{-1}$ = $L_6 (T_x/6 \text{ kev})^\alpha (1+z)^A$ where A is predicted to be $-0.7 < A < 0.7$ in ICM models with additional entropy from non-gravitational sources of heating (Tozzi & Norman 2001) while $A = 1.5$ in self-similar models. We find $A = 0.41 \pm 0.21$, when comparing our whole $z > 0.7$ sample with Arnaud & Evrard (1999) and, similarly $A = 0.27 \pm 0.22$ when comparing with Markevitch (1998). Though our results cannot accurately pin down the value of A , we can rule out at the 5σ level the evolution predicted for self-similar ICM model. Both of the values for A we have above are lower than the value of 0.60 ± 0.38 found by Fairley et al. (2000), though not by more than one standard deviation.

Mushotzky & Scharf (1997) constructed two samples, a $z < 0.1$ sample and a $z > 0.14$ sample with a characteristic redshift of $z \simeq 0.3$. Mushotzky & Scharf (1997) find no observed evolution with $A = 0.0 \pm 0.7$. The agreement in the observed lack of evolution between a variety of different samples observed with different instruments, solidifies the evidence that the self-similar scaling model cannot explain ICM formation. Moreover, a value of A close to zero implies little evolution of the cluster temperature (or mass) function based on the observed mild evolution of the X-ray luminosity function. As discussed in Borgani et al. (2001b), this result strongly points toward low values of Ω_m .

Two of the objects in our sample, RDCS0848+4453 and CDFS-CL1, have temperatures and luminosities near the group/cluster boundary. As discussed in the introduction, low temperature clusters and groups have much lower binding masses and so should show greater evidence of non-gravitational sources of heating. Therefore, to rigorously test pre-heating models of ICM formation will require more objects at these temperatures and luminosities. Surveys such as **Chandra** Multi-wavelength Project (ChaMP) (Wilkes et al. 2000) and the proposed XMM survey of Romer et al. (2001) will provide the necessary follow-up of deep X-ray pointings to find the low luminosity, low X-ray temperature yet high redshift clusters and groups. In Figure 13 we show an example of one such object, the new X-ray group, CXOU J0910.1+5419. This is one of the two systems, detailed in the Appendix, that we found serendipitously in our **Chandra** pointings. In four fields, roughly 0.4 square degrees, we have found two low temperature cluster/groups. ChaMP and the XMM survey of Romer et al. (2001) should find on the order ten or so objects a year with these temperatures at $z \simeq 0.5$. Such a sample will be ideally suited for studying the evolution of the intracluster/intragroup medium luminosity-temperature relation for low mass systems, the same

systems for which pre-heating models predict the strongest effects.

6. Summary

We report the discovery and follow-up observations for RDCS1317+2911 and RDCS1350+6007, two clusters of galaxies found in the **ROSAT** Deep Cluster Survey (RDCS). RDCS1317+2911, which we find at $z = 0.805$, appears to have a highly elliptical, non-axisymmetric X-ray surface brightness profile based on our **Chandra** images. RDCS1317+2911 is poorly described by a β model, implying that either we are observing a newly forming cluster, or a recent merger event. Our best fitting temperature is $3.7_{-0.9}^{+1.5}$ keV with a bolometric luminosity of $8.2_{-1.6}^{+1.7} \times 10^{43}$ erg s $^{-1}$. RDCS1350+6007, at a $z = 0.804$, appears asymmetric as well, but has the conventional β model parameters of $\beta = 0.49 \pm 0.06$ and $r_{core} = 165 \pm 5$ kpc. We estimate a temperature $4.9_{-0.9}^{+1.6}$ keV and a bolometric luminosity of $4.1_{-0.4}^{+0.5} \times 10^{44}$ erg s $^{-1}$ for RDCS1350+6007.

RDCS1350+6007 has a strong weak lensing signal. Our weak lensing mass estimate is twice that of the mass we derive from the X-ray temperature and surface brightness profile. We speculate that we are observing a merging cluster. A merger along the line of sight would have a larger total mass in the weak lensing results than implied by the assumption of hydrostatic equilibrium for the X-ray emitting gas. Such an event could also serve to heat up the gas, breaking hydrostatic equilibrium. Thus, we could be underestimating the true slope of the gas profile, and therefore, the depth, of the potential well.

We combine the two temperature and luminosity measurements in this paper with other high redshift cluster X-ray temperature and luminosities from the literature and create a sample with $z_{median} = 0.83$. We find with this sample a luminosity-temperature relation of the form $L_x = L_6 \left(\frac{T}{6\text{keV}} \right)^\alpha$ where $L_6 = 8.7 \pm 0.9 \times 10^{44}$ erg s $^{-1}$ and $\alpha = 2.9 \pm 0.4$. Our results agree with the low redshift luminosity-temperature relations (Allen & Fabian 1998; Markevitch 1998; Arnaud & Evrard 1999). If we parameterize the evolution in the relation as $L_{x,bol} \text{ erg s}^{-1} = L_6 (T_x/6 \text{ kev})^\alpha (1+z)^A$, we find $A = 0.3 - 0.4 \pm 0.2$ depending on which low redshift sample we compare against. Such evolution agrees with other measurements, such as $A = 0.6 \pm 0.4$ by Fairley et al. (2000) and $A = 0.0 \pm 0.7$ by Mushotzky & Scharf (1997). The agreement between all of these measurements provide convincing evidence that there is little or no evolution in the luminosity-temperature relation. This provides more weight for ICM evolution models that require significant additional entropy beyond gravitational heating.

We thank Maxim Markevitch for assistance with planning our **Chandra** observation. We thank Dan Stern for providing us with the LRIS spectral reduction routines. We wish to thank the anonymous referee for useful comments and criticisms. Support for SAS came from NASA/LTSA grant NAG5-8430 and for BH from NASA/Chandra GO0-1082A. Both BH and SAS are supported by the Institute for Geophysics and Planetary Physics (operated under the auspices of the US

Department of Energy by the University of California Lawrence Livermore National Laboratory under contract W-7405-Eng-48). Support for GKS in this work was provided by NASA through Hubble Fellowship Grant No. HF-01114.01-98A from the Space Telescope Science Institute, which is operated by the Association of Universities for Research in Astronomy, Incorporated, under NASA Contract NAS5-26555. Some of the data presented herein were obtained at the W.M. Keck Observatory, which is operated as a scientific partnership among the California Institute of Technology, the University of California and the National Aeronautics and Space Administration. The Observatory was made possible by the generous financial support of the W.M. Keck Foundation. The authors wish to extend special thanks to those of Hawaiian ancestry on whose sacred mountain we are privileged to be guests. Without their generous hospitality, many of the observations presented herein would not have been possible.

A. The Discovery of Two X-ray Groups: CXOU J0910.1+5419 and CXOU J1316.9+2914

We report the discovery of two new X-ray emitting groups or low mass clusters of galaxies. Both systems, CXOU J0910.1+5419 and CXOU J1316.9+2914, were found as extended X-ray sources in our Chandra images. Though we mention these in the text of the paper, here we will detail their properties.

In our observation of RDCS1317+2911, we also found CXOU J1316.9+2914, a low redshift, group of galaxies visible on the Digitized Sky Survey found at $\alpha = 13h 16m 54.2s$ $\delta = 29^\circ 14' 15''$ (J2000). We extracted a nearby background region and use the same model for the background as for RDCS1317+2911. We found a net of 174.5 events inside the aperture for CXOU J1316.9+2914 to which we fit a Raymond-Smith model. The group has a $z = 0.42_{-0.10}^{0.14}$, $T_x = 2.9_{-1.2}^{+3.1}$ keV with a flux of $6.7_{-1.0}^{+1.0} \times 10^{-15}$ ergs cm $^{-2}$ s $^{-1}$ (0.5-2.0 keV). Given the large errors on the redshift it is certainly consistent with the gas being associated with the group of galaxies and not with a higher redshift system along the line of sight.

We also found CXOU J0910.1+5419 in examining the X-ray data in Stanford et al. (2002). This object is interesting in that it possesses a hard X-ray core, possibly the result of an active galactic nuclei at the cluster center but with no apparent counterpart. In Figure 13 we show the registered infrared data, obtained at the Mayall 4m using the SQIID, with the X-ray data as contours. We registered the infrared and X-ray data separately with the Digitized Sky Survey⁹. We found a small offset of 1'' in both right ascension and in declination between the X-ray data and the Digitized Sky Survey data, the same that was found for RDCS0910+5422 in Stanford et al. (2002).

⁹The Digitized Sky Survey was produced at the Space Telescope Science Institute under U.S. Government grant NAG W-2166. The images of these surveys are based on photographic data obtained using the Oschin Schmidt Telescope on Palomar Mountain and the UK Schmidt Telescope. The plates were processed into the present compressed digital form with the permission of these institutions.

Within $30''$ of the center, $\alpha = 09h\ 10m\ 08\overset{s}{.}6$ $\delta = 54^\circ 18' 56\overset{''}{.}3$ (J2000), with the central $5''$ removed, we found 464 events over 0.5-6.0 keV with 196.6 expected from the background in the same energy range. We used the same functional form for the background model as used in Stanford et al. (2002). The fit to the background yielded the same parameters. We fit a Raymond-Smith model with a metal abundance fixed at 0.3 solar to those events with the background model fixed. The most likely result we found was $z = 0.68 \pm 0.06$ and $T_x = 2.0 \pm 0.5$ keV. The maximum likelihood distribution is almost bimodal with a second peak with $z = 1.18^{+0.08}_{-0.07}$ and $T_x = 2.5^{+0.6}_{-0.5}$ keV. These are the 68% confidence limits as determined from 1000 Monte Carlo simulations for each set of input values. If we look at the overall distribution of likelihood values, however, we see that there is large degeneracy between the redshift and temperature for this object. Thus, the 95% confidence limits encompass both combinations of redshift and temperature and all values in between. The observed infrared colors are more consistent with the lower redshift, however, so we will chose that value as the most likely. The flux inside the aperture was $7.3^{+0.6}_{-0.6} \times 10^{-15}$ ergs $\text{cm}^{-2} \text{ s}^{-1}$ (0.5-2.0 keV) and $9.6^{+1.0}_{-1.0} \times 10^{-15}$ ergs $\text{cm}^{-2} \text{ s}^{-1}$ (0.5-6.0 keV) for both temperatures, making the object almost as bright as RDCS1317+2911 in terms of flux, but slightly harder.

REFERENCES

Akritas, M. G. & Bershady, M. A. 1996, ApJ, 470, 706

Allen, S. W. & Fabian, A. 1998, MNRAS, 297, L57

Arnaud, K. A. 1996, in ASP Conference Series, Vol. 101, Astronomical Data Analysis Software and Systems V, ed. G. Jacoby & J. Barnes, 17

Arnaud, M. & Evrard, A. E. 1999, MNRAS, 305, 631

Böhringer, H., Soucail, G., Mellier, Y., Ikebe, Y., & Schuecker, P. 2000, A&A, 353, 124

Beers, T. C., Flynn, K., & Gebhardt, K. 1990, AJ, 100, 32

Bertin, E. & Arnouts, S. 1996, A&AS, 117, 393

Bialek, J. J., Evrard, A. E., & Mohr, J. J. 2001, ApJ, 555, 597

Borgani, S., Governato, F., Wadsley, J., Menci, N., Tozzi, P., Lake, G., Quinn, T., & Stadel, J. 2001a, ApJ, 559, L71

Borgani, S., Rosati, P., Tozzi, P., Stanford, S. A., Eisenhardt, P., Lidman, C., Holden, B., Norman, C., & Squires, G. 2001b, ApJ, 561, 13

Bower, R. G., Castander, F. J., Couch, W., Ellis, R. S., & Böhringer, H. 1997, MNRAS, 291, 353

Cagnoni, I., Elvis, M., Kim, D.-W., Mazzotta, P., Huang, J.-S., & Celotti, A. 2001, ApJ, 560, 86

Cash, W. 1979, *ApJ*, 228, 939

Cavaliere, A., Menci, N., & Tozzi, P. 1997, *ApJ*, 484, L21

—. 1999, *MNRAS*, 308, 599

Czoske, O., Kneib, J.-P., Soucail, G., Bridges, T. J., Mellier, Y., & Cuillandre, J.-C. 2001, *A&A*, 372, 391

Della Ceca, R., Scaramella, R., Gioia, I., Rosati, P., Fiore, F., & Squires, G. 2000, *A&A*, 353, 498

Donahue, M., Voit, G. M., Scharf, C. A., Gioia, I. M., Mullis, C. R., Hughes, J. P., & Stocke, J. T. 1999, *ApJ*, 527, 525

Ebeling, H., Jones, L. R., Fairley, B. W., Perlman, E., Scharf, C., & Horner, D. 2001, *ApJ*, 548, L23

Edge, A. C. & Stewart, G. C. 1991, *MNRAS*, 252, 414

Ellis, T., Drake, R., Fowler, A. M., Gatley, I., Heim, J., Luce, R., Merrill, K. M., Probst, R., & Bucholz, N. 1992, *Proc. SPIE*, 1765, 94

Evrard, A. E. & Henry, J. P. 1991, *ApJ*, 383, 95

Fabricant, D., Rybicki, G. B., & Gorenstein, P. 1984, *ApJ*, 286, 186

Fahlman, G., Kaiser, N., Squires, G., & Woods, D. 1994, *ApJ*, 437, 56

Fairley, B. W., Jones, L. R., Scharf, C., Ebeling, H., Perlman, E., Horner, D., Wegner, G., & Malkan, M. 2000, *MNRAS*, 315, 669

Fernández-Soto, A., Lanzetta, K. M., & Yahil, A. 1999, *ApJ*, 513, 34

Freeman, P. E., Doe, S., & Siemiginowska, A. 2001, in *Astronomical Data Analysis Software and Systems X*, ASP Conference Proceedings, Vol. 238. Edited by F. R. Harnden, Jr., Francis A. Primini, and Harry E. Payne. San Francisco: Astronomical Society of the Pacific, ISSN: 1080-7926, 2001., p.483, Vol. 10, 483+

Giacconi, R., Zirm, A., Wang, J., Rosati, P., Nonino, M., Tozzi, P., Gilli, R., Mainieri, V., Hasinger, G., Kewley, L., Bergeron, J., Borgani, S., Gilmozzi, R., Grogan, N., Koekemoer, A., Schreier, E., Zheng, W., & Norman, C. 2001, *ApJS*, accepted, astro

Gioia, I. M., Henry, J. P., Maccacaro, T., Morris, S. L., Stocke, J. T., & Wolter, A. 1990, *ApJ*, 356, 35

Gioia, I. M., Henry, J. P., Mullis, C. R., Ebeling, H., & Wolter, A. 1999, *AJ*, 117, 2608

Gioia, I. M. & Luppino, G. A. 1994, *ApJS*, 94, 583

Gorenstein, M. V., Shapiro, I. I., & Falco, E. E. 1988, *ApJ*, 327, 693

Gwyn, S. D. J. 1999, <http://astrowww.phys.uvic.ca/grads/gwyn/pz/index.html>

Gwyn, S. D. J. & Hartwick, F. D. A. 1996, *ApJ*, 468, 77

Hashimoto, Y., Hasinger, G. ., Arnaud, M., Rosati, P., & Miyaji, T. 2002, *A&A*, 381, 841

Helsdon, S. F. & Ponman, T. J. 2000, *MNRAS*, 315, 356

Henry, J. P., Briel, U. G., & Nulsen, P. E. J. 1993, *A&A*, 271, 413

Henry, J. P., Gioia, I., Maccacaro, T., Morris, S. L., Stocke, J., & Wolter, A. 1992, *ApJ*, 386, 408

Hoekstra, H., Franx, M., Kuijken, K., & Squires, G. 1998, *ApJ*, 504, 636

Holden, B. P., Stanford, S. A., Rosati, P., Squires, G., Tozzi, P., Fosbury, R. A. E., Papovich, C., Eisenhardt, P., Elston, R., & Spinrad, H. 2001, *AJ*, 122, 629

Horner, D., Baumgartner, W., Mushotzky, R., & Gendreau, K. 2001, in *BAAS*, Vol. 199, 10021

Jarrett, T. H., Beichman, C. A., van Buren, D., Gautier, N., Jorquera, C., & Bruce, C. 1994, *Experimental Astronomy*, 3, 133

Jeltema, T. E., Canizares, C. R., Bautz, M. W., Malm, M. R., Donahue, M., & Garmire, G. P. 2001, *ApJ*, 562, 124

Jones, C. & Forman, W. 1999, *ApJ*, 511, 65

Kaiser, N. 1986, *MNRAS*, 222, 323

—. 1991, *ApJ*, 383, 104

Kaiser, N., Squires, G., & Broadhurst, T. 1995, *ApJ*, 449, 460

Kells, W., Dressler, A., Sivaramakrishnan, A., Carr, D., Koch, E., Epps, H., Hilyard, D., & Pardeihan, G. 1998, *PASP*, 110, 1487

Lloyd-Davies, E. J., Ponman, T. J., & Cannon, D. B. 2000, *MNRAS*, 315, 689

Loewenstein, M. 2000, *ApJ*, 532, 17

Luppino, G. A. & Kaiser, N. 1997, *ApJ*, 475, 20

Markevitch, M. 1998, *ApJ*, 504, 27

Mushotzky, R. F. & Scharf, C. A. 1997, *ApJ*, 482, L13

O'dell, S. L. & Weisskopf, M. C. 1998, in *Proc. SPIE* Vol. 3444, p. 2-18, *X-Ray Optics, Instruments, and Missions*, Richard B. Hoover; Arthur B. Walker; Eds., Vol. 3444, 2-18

Oke, J. B., Cohen, J. G., Carr, M., Cromer, J., Dingizian, A., Harris, F. H., Labrecque, S., Lucinio, R., Schaal, W., Epps, H., & Miller, J. 1995, PASP, 107, 375

Ponman, T. J., Cannon, D. B., & Navarro, J. F. 1999, Nature, 397, 135

Raymond, J. C. & Smith, B. W. 1977, ApJS, 35, 419

Romer, A. K., Viana, P. T. P., Liddle, A. R., & Mann, R. G. 2001, ApJ, 547, 594

Rosati, P., Della Ceca, R., Norman, C., & Giacconi, R. 1998, ApJ, 492, L21

Smail, I., Ellis, R. S., Dressler, A., Couch, W. J., Oemler, A. J., Sharples, R. M., & Butcher, H. 1997, ApJ, 479, 70+

Stanford, S. A., Holden, B., Rosati, P., Tozzi, P., Borgani, S., Eisenhardt, P. R., & Spinrad, H. 2001, ApJ, 552, 504

Stanford, S. A., Holden, B. P., Rosati, P., Eisenhardt, P. R., Stern, D., Squires, G., & Spinrad, H. 2002, AJ, 123, 619

Stark, A. A., Gammie, C. F., Wilson, R. W., Balley, J., Linke, R. A., Heiles, C., & Hurwity, M. 1992, ApJS, 79, 77

Tozzi, P. & Norman, C. 2001, ApJ, 546, 63

Tyson, J. A., Kochanski, G. P., & dell'Antonio, I. P. 1998, ApJ, 498, L107

Vikhlinin, A. 2001, http://hea-www.harvard.edu/~alexey/vf_bg/vfbg.html

Voit, M. & Bryan, G. 2001, Nature, 414, 425

White, R. E. 1991, ApJ, 367, 69

Wilkes, B., Green, P., Cameron, R., Evans, N., Ghosh, H., Kim, D. W., Tananbaum, H., & ChaMP Collaboration. 2000, AAS/High Energy Astrophysics Division, 32, 2105

Wu, K. K. S., Fabian, A. C., & Nulsen, P. E. J. 2000, MNRAS, 318, 889

Zaroubi, S., Squires, G., de Gasperis, G., Evrard, A. E., Hoffman, Y., & Silk, J. 2001, ApJ, 561, 600

Zaroubi, S., Squires, G., Hoffman, Y., & Silk, J. 1998, ApJ, 500, L87

Fig. 1.— A three-color montage of RDCS1317+2911 with the 0.5-2.0 keV X-ray data, smoothed with a $3''$ Gaussian, overlaid as green contours. The blue color is from a Gunn i band image, with green and red from J and K_s band imaging. The image is $2.5''$ by $2.5''$ on a side and the lowest contour level is 4σ above the background. The image in the upper right shows the 2.0-10.0 keV X-ray data smoothed with the same Gaussian. The hard point source seen in the inset is discussed in §2.3.

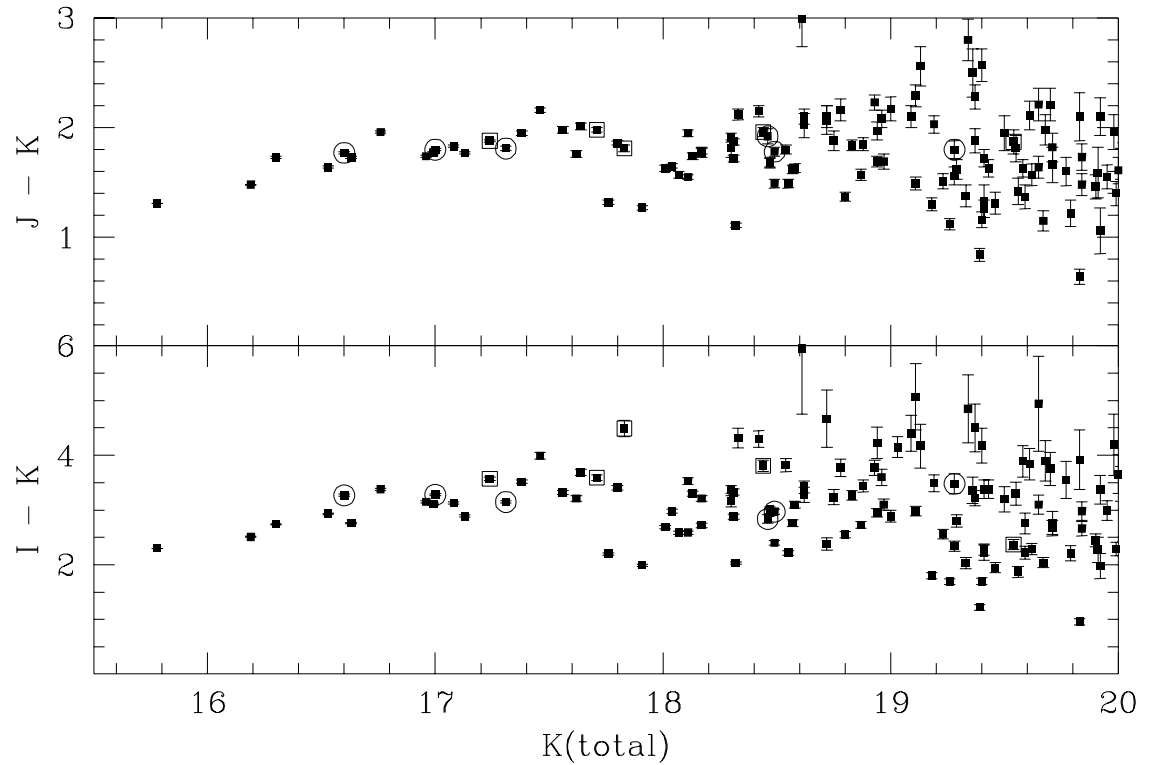


Fig. 2.— The color-magnitude diagrams for RDCS1317+2911. See §2.1 for details on how the photometry was constructed. The circled points represent spectroscopically confirmed cluster members while the points with squares represent galaxies not at the redshift of the cluster.

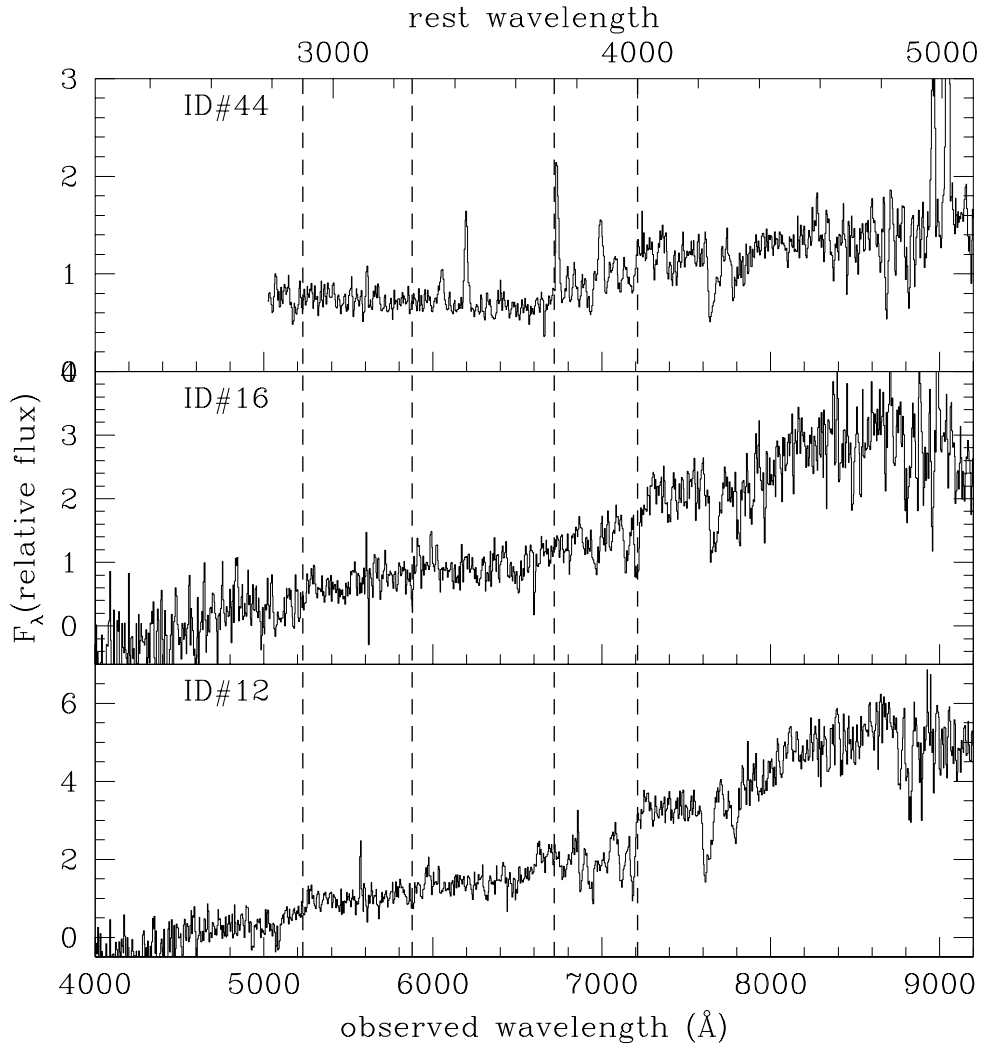


Fig. 3.— We plot spectra for three of the members of RDCS1317+2911. Each spectrum is shifted to the rest frame of the cluster. The four vertical dashed lines represent the break at 2900 Å, the break at 3260 Å, O II at 3727 Å, and the break at 4000 Å. ID #44, at the top, shows evidence of O III at 4959 Å and 5007Å.

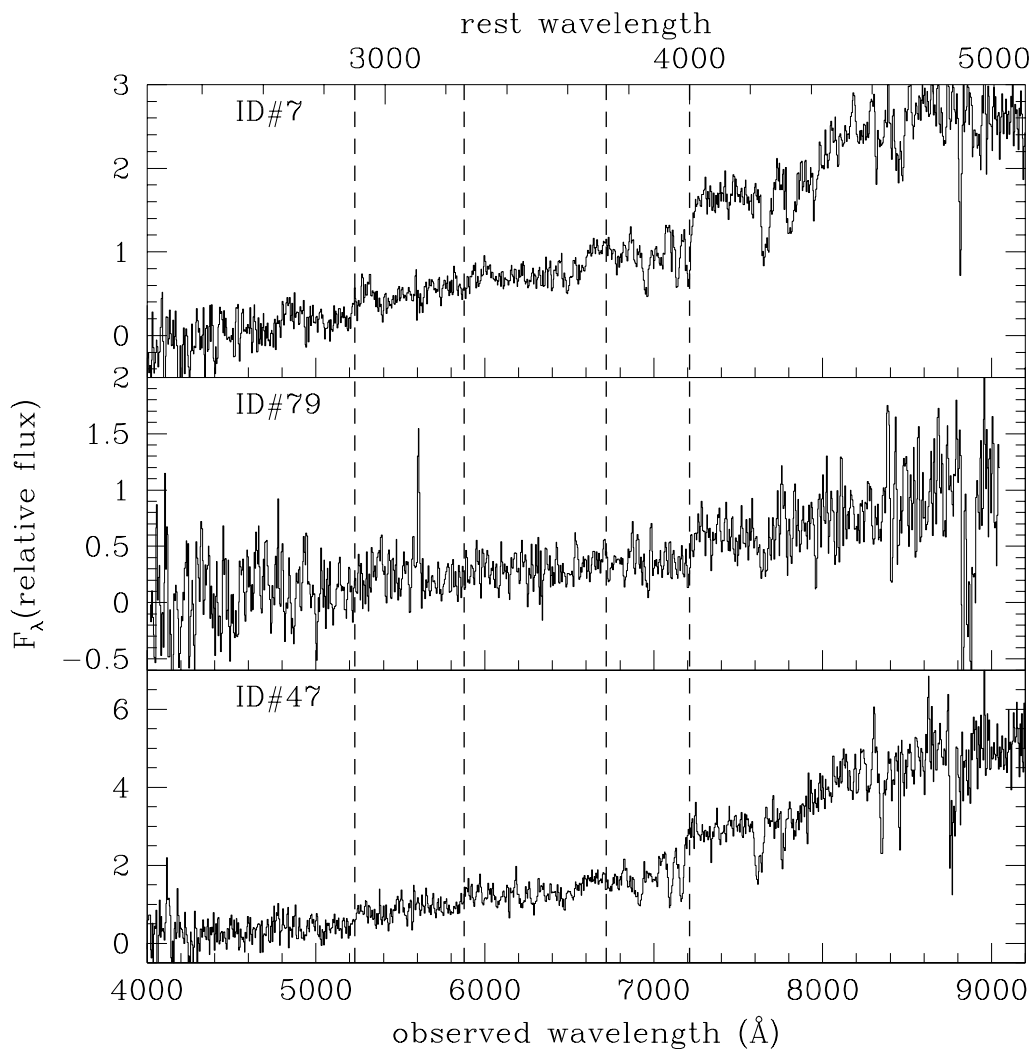


Fig. 4.— See Figure 3.

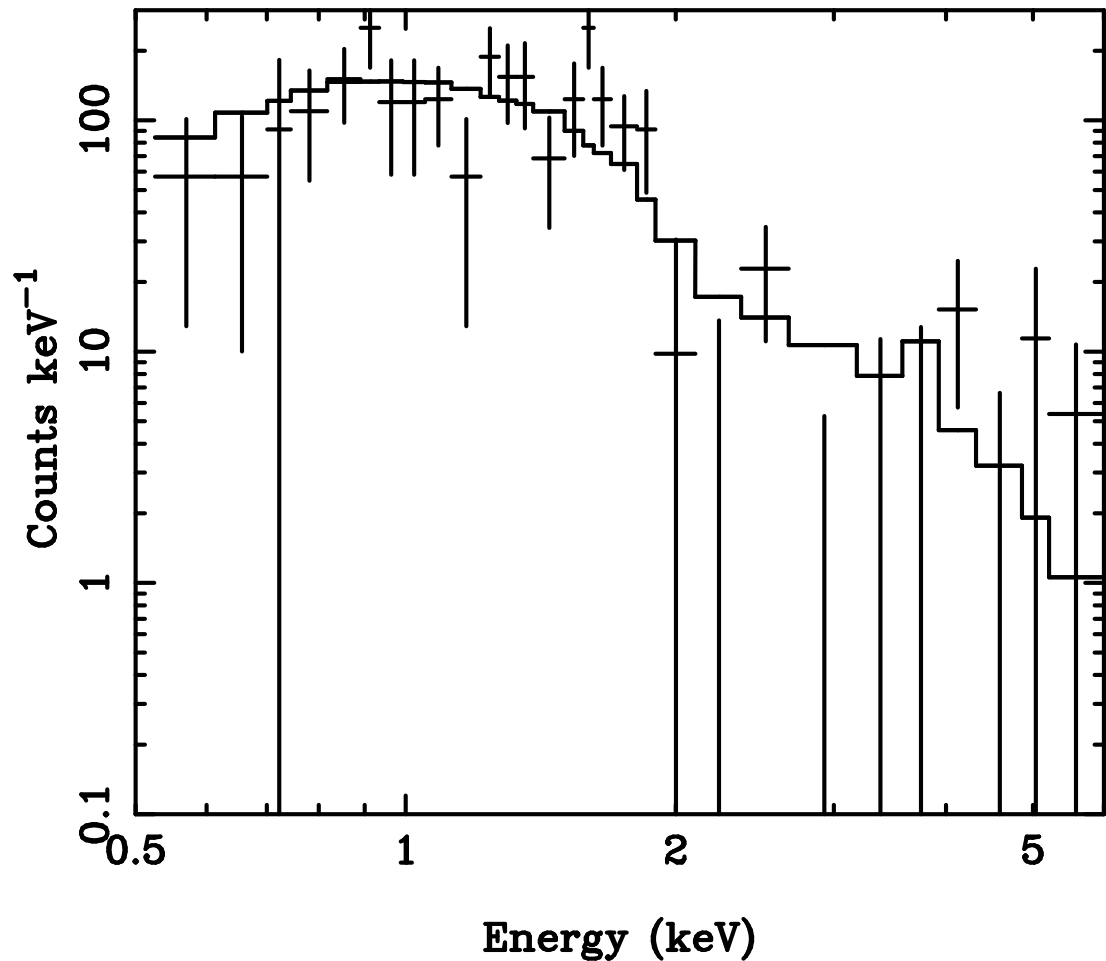


Fig. 5.— Our best fitting spectrum for RDCS1317+2911 with the background model subtracted and the data grouped into bins of 10 events each.

Fig. 6.— RDCS1350+6007 with the 0.5-2.0 keV X-ray data, smoothed with a $3''$ Gaussian, overlaid as green contours on top of an three-color image. The blue color is from an R band image, with green from an J band image and the K_s image for the red component. The field size is $2'3$ by $2'3$ with the lowest contour at 5σ of the background.

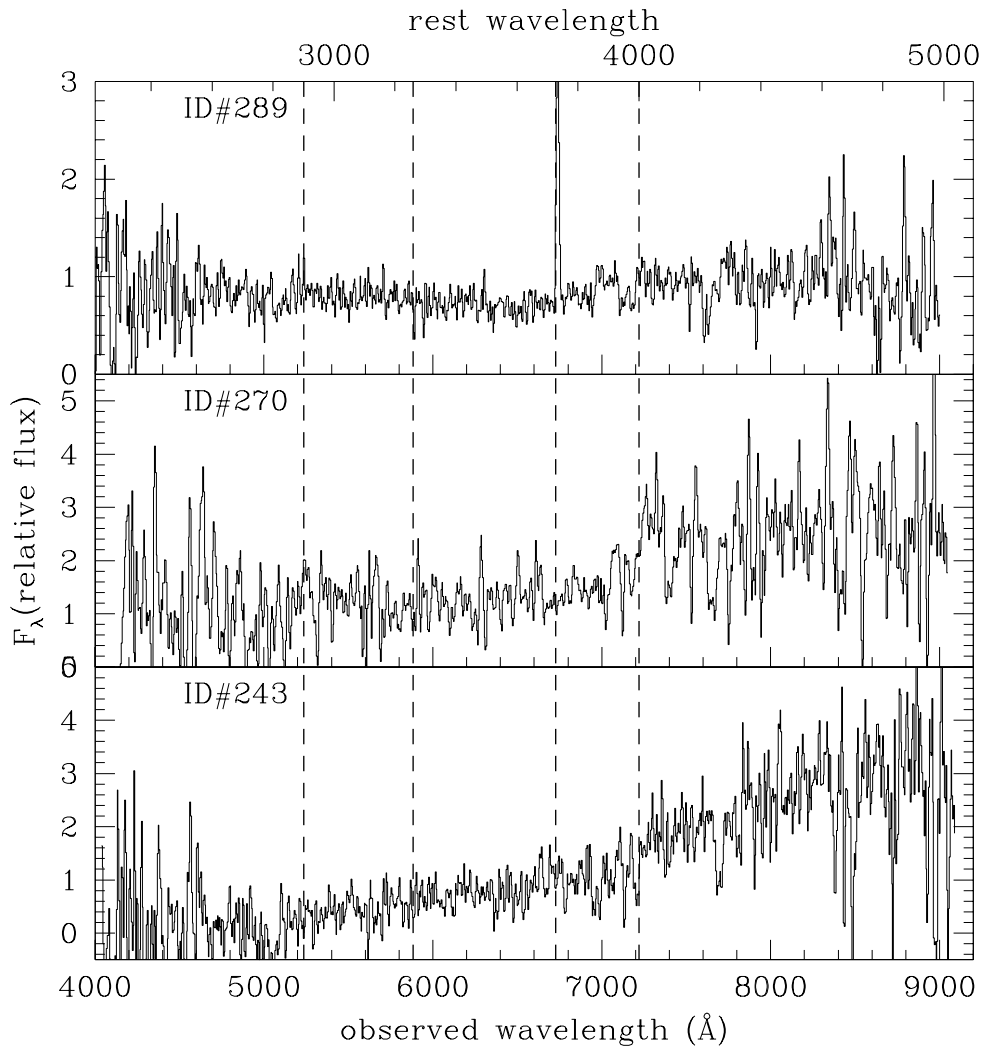


Fig. 7.— We plot spectra for three of the members of RDCS1350+6007 in the cluster rest-frame. The vertical lines are the same as in Figure 3.

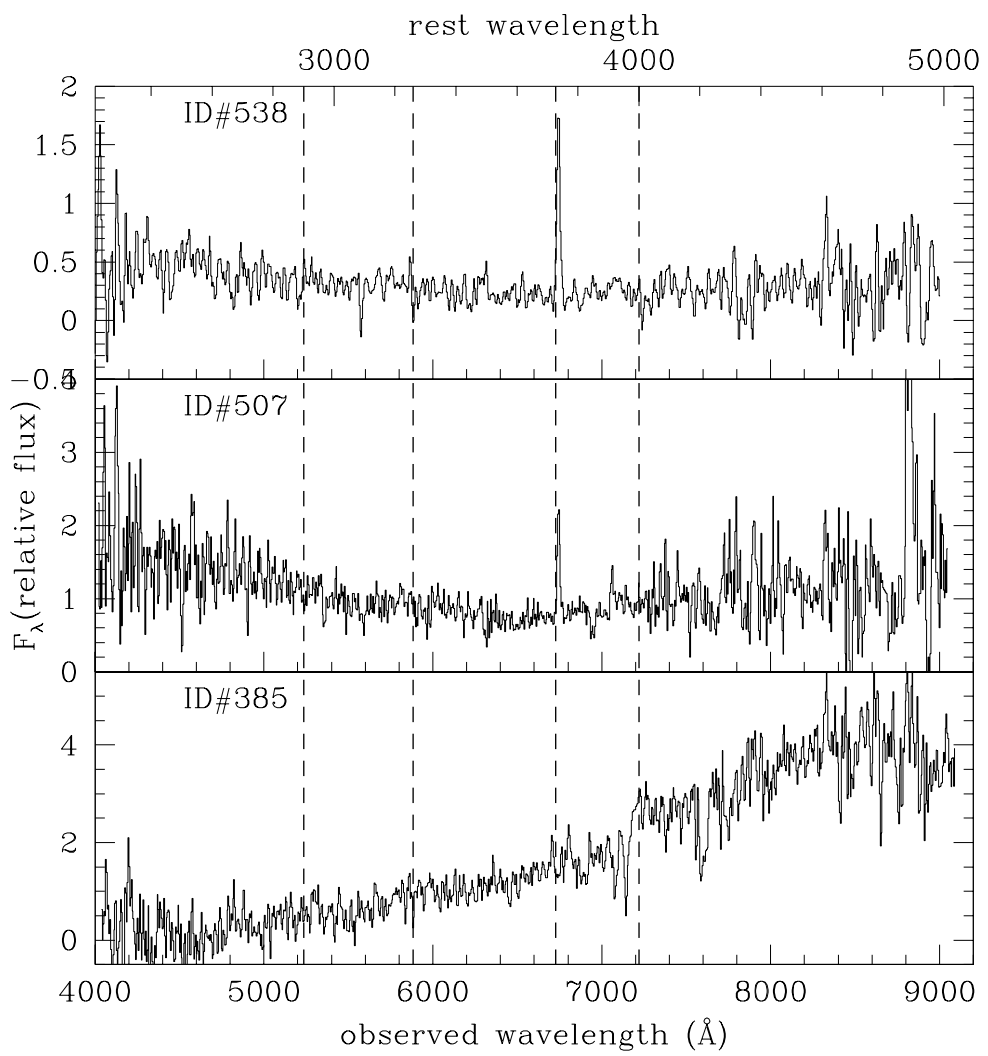


Fig. 8.— See Figure 7.

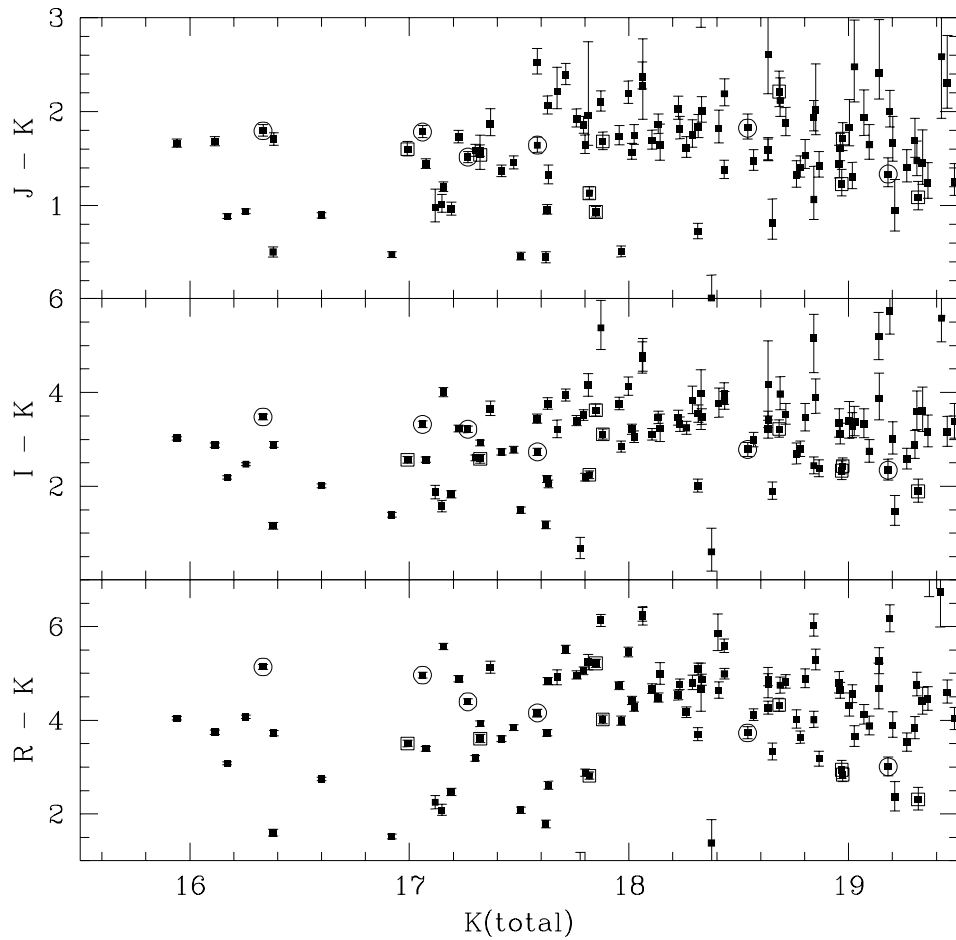


Fig. 9.— The color-magnitude diagrams for RDCS1350+6007. See §2.2 for details on how the photometry was constructed. The circled points represent spectroscopically confirmed cluster members while the points with squares are non-cluster members.

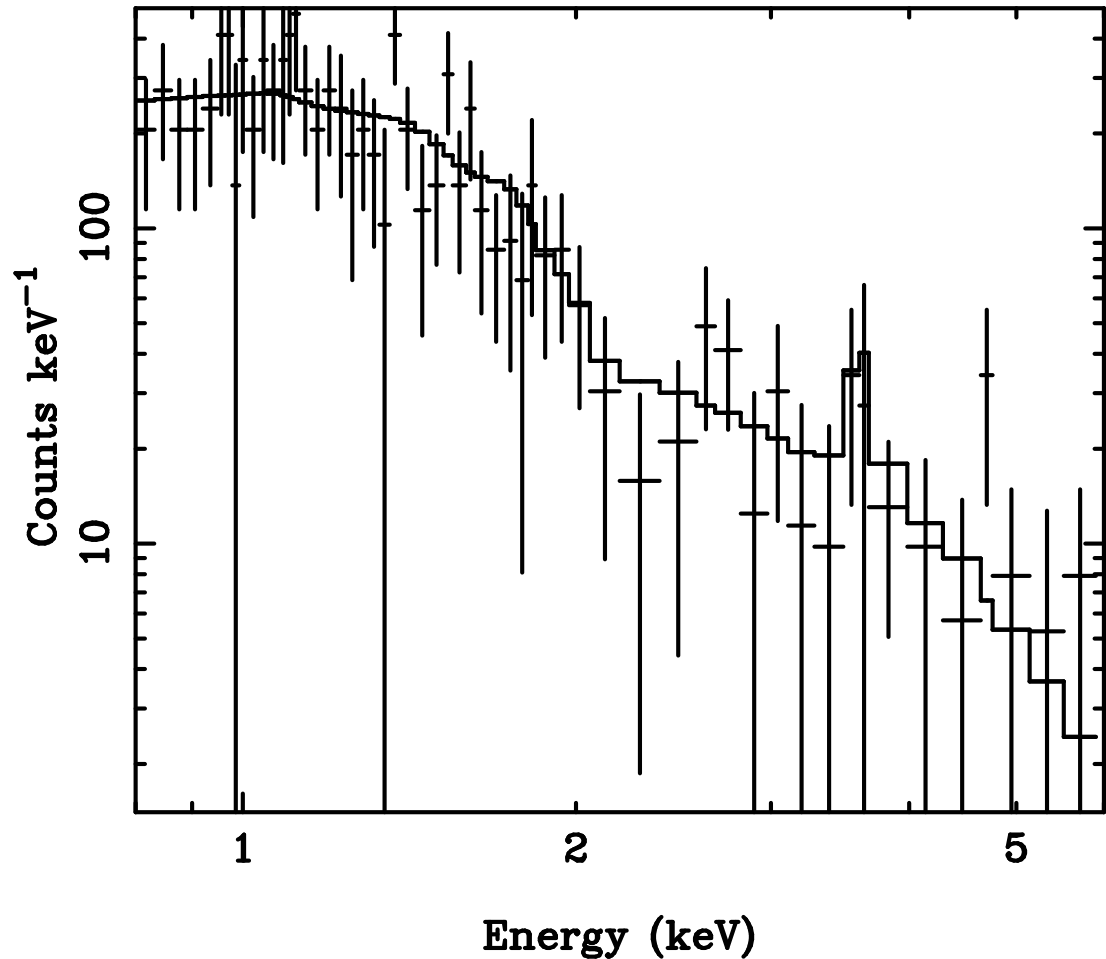


Fig. 10.— Our best fitting spectrum for RDCS1350+6007 with the background model subtracted and the data grouped into bins of five events each.

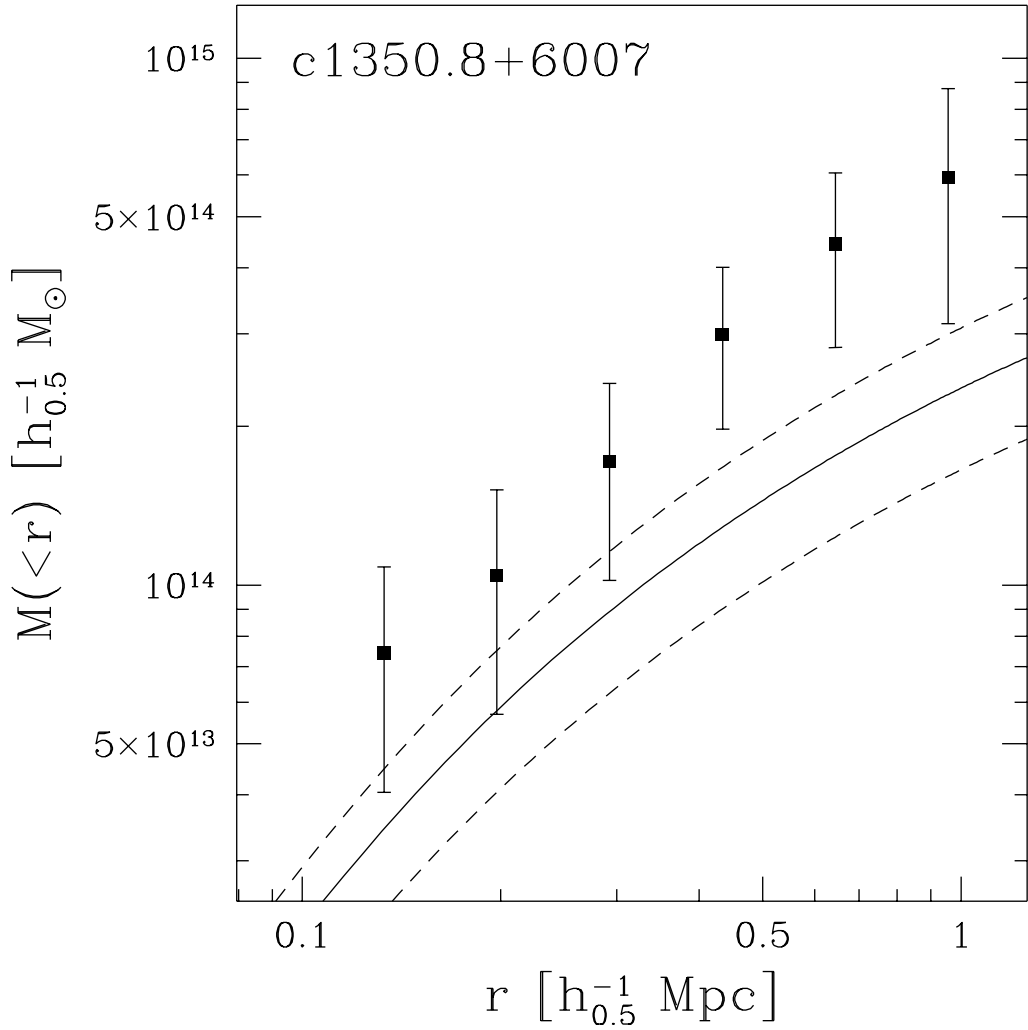


Fig. 11.— The total enclosed mass as a function of projected distance from the cluster center. The solid line represents the enclosed mass based on assuming an isothermal gas following the β model distribution and the dashed lines represent the 68% confidence limits for that model. The points are the enclosed mass measurements from the weak lensing analysis. Each weak lensing data point represents the cumulative mass inside that aperture, so the errors are correlated between the data points.

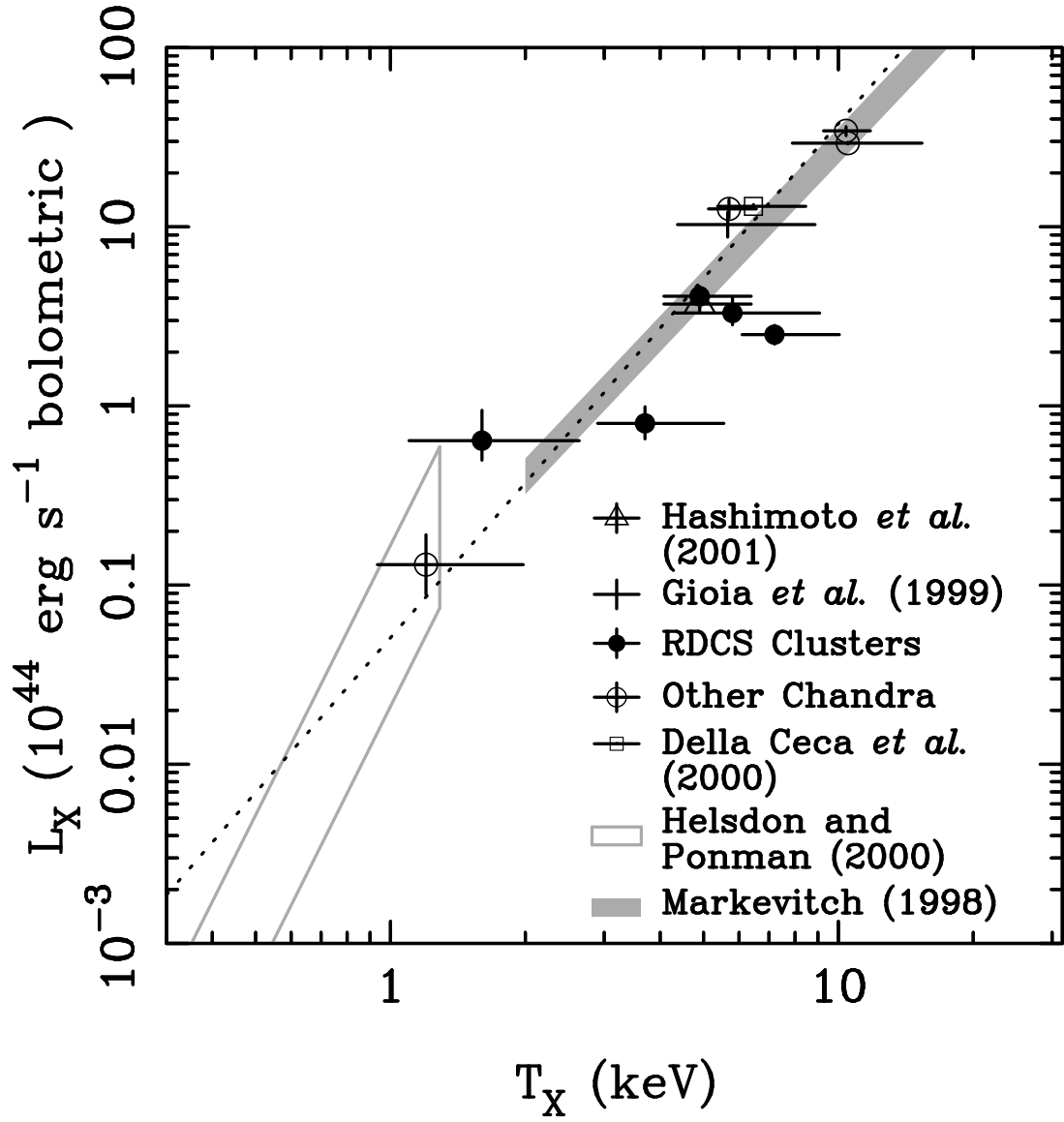


Fig. 12.— The luminosity-temperature relation discussed in this paper. Low redshift group data, represented by asterisks, are from Helsdon & Ponman (2000). The low redshift cluster results, from Markevitch (1998), are plotted as the shaded region. All other clusters are at $z > 0.7$ and the dotted line represents the fit to that sample given in the text.

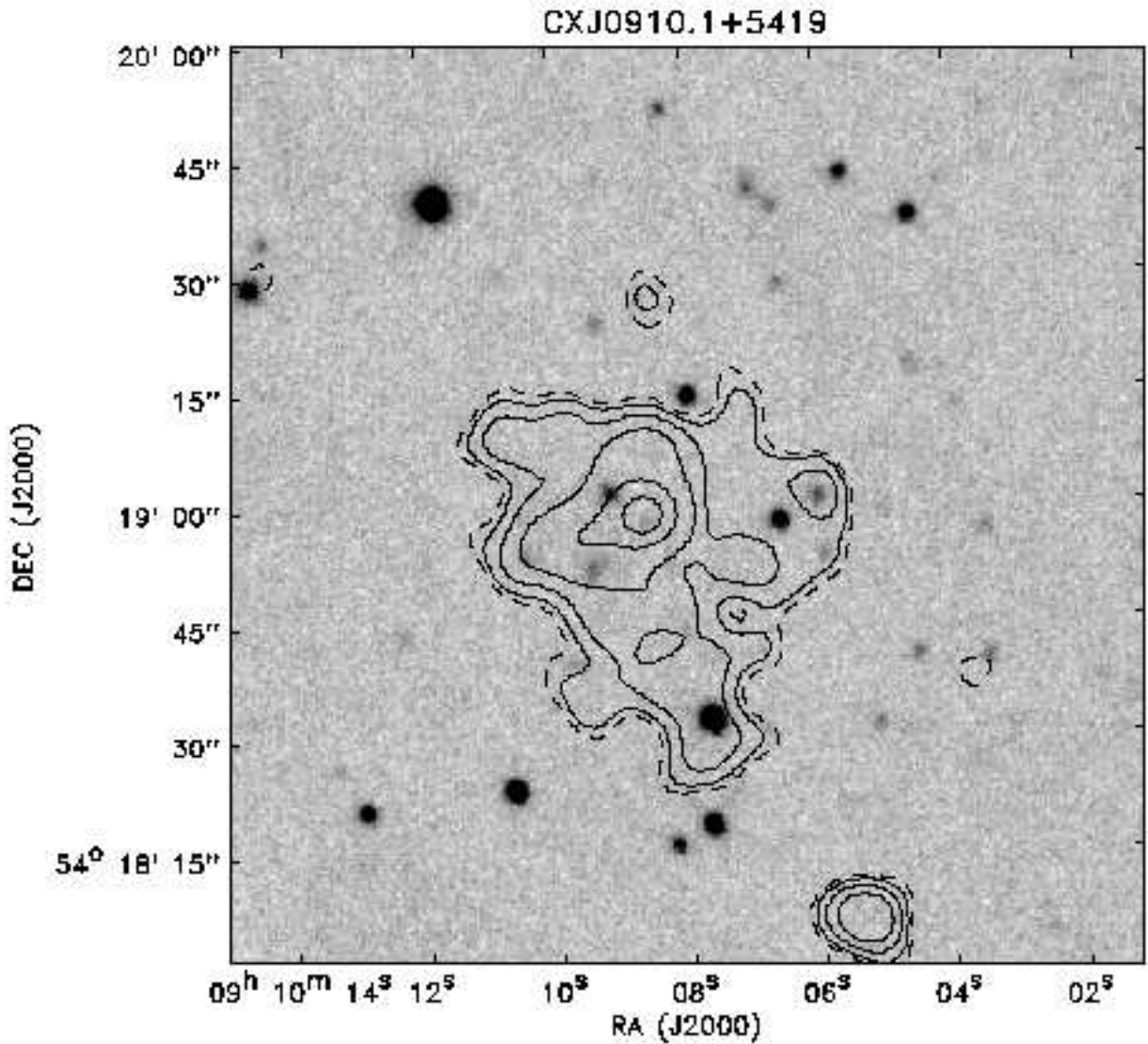


Fig. 13.— An image of CXOU J0910.1+5419 taken with the Simultaneous Quad IR Imaging Device on the KPNO Mayall 4 meter telescope. The data are both the J and K_s registered and summed. Plotted with contours is the 0.5-2.0 keV X-ray data smoothed with a $3''$ Gaussian. The lowest contour level represents a 4σ variation in the background counts.

Table 1. Results from $z > 0.7$ Clusters of Galaxies

Name	z	Luminosity (bol., 10^{44} erg s $^{-1}$)	kT (keV)	Refs.
RDCS0849+4452	1.273	$0.64^{+0.25}_{-0.16}$	$1.6^{+0.8}_{-0.6}$	1
RDCS0848+4453	1.261	$3.3^{+0.7}_{-0.5}$	$5.8^{+2.6}_{-1.7}$	1
RDCS0910+5422	1.101	$2.5^{+0.3}_{-0.3}$	$7.2^{+2.4}_{-1.2}$	2
RDCS1317+2911	0.805	$0.82^{+0.17}_{-0.16}$	$3.7^{+1.5}_{-0.9}$	
RDCS1350+6007	0.804	$4.1^{+0.5}_{-0.4}$	$4.9^{+1.3}_{-0.9}$	
CDFS-CL1	0.73	$0.13^{+0.05}_{-0.05}$	$1.2^{+0.6}_{-0.3}$	3
MS1137.5+6625	0.782	$12.6^{+1.5}_{-1.5}$	$5.7^{+0.8}_{-0.6}$	4,5,6
RX J1716+6708	0.813	$10.3^{+0.5}_{-0.5}$	$5.7^{+2.5}_{-1.5}$	7
MS1054.4+0321	0.833	$34.3^{+1.9}_{-2.1}$	$10.4^{+1.3}_{-1.2}$	8
RDCS0152.7-1357	0.831	$13.0^{+0.3}_{-0.3}$	$6.5^{+1.7}_{-1.2}$	9
1WGA J1226.9+3332	0.89	$29.3^{+3.0}_{-3.0}$	$10.5^{+4.0}_{-3.0}$	10
RX J1053.7+5753	1.26	$3.4^{+0.34}_{-0.34}$	$4.9^{+1.3}_{-0.9}$	11

References. — (1) Stanford et al. (2001); (2) Stanford et al. (2002); (3) Giacconi et al. (2001); (4) Borgani et al. (2001b); (5) Gioia & Luppino (1994); (6) Donahue et al. (1999); (7) Gioia et al. (1999); (8) Jeltema et al. (2001); (9) Della Ceca et al. (2000); (10) Cagnoni et al. (2001); Ebeling et al. (2001); (11) Hashimoto et al. (2002)

This figure "holden.fig1.jpg" is available in "jpg" format from:

<http://arxiv.org/ps/astro-ph/0203474v2>

This figure "holden.fig6.jpg" is available in "jpg" format from:

<http://arxiv.org/ps/astro-ph/0203474v2>